



HAL
open science

Development of a Novel Self-locking-at-rest Piezoelectric Inchworm Motor with High Switching Frequency Driving Ability

Sandip Jana, Sofiane Ghenna, Saikat Kumar Shome, Yves Bernard, Arup Kumar Nandi, Laurent Daniel

► To cite this version:

Sandip Jana, Sofiane Ghenna, Saikat Kumar Shome, Yves Bernard, Arup Kumar Nandi, et al.. Development of a Novel Self-locking-at-rest Piezoelectric Inchworm Motor with High Switching Frequency Driving Ability. Precision Engineering, 2025, 10.1016/j.precisioneng.2025.01.027 . hal-04930862

HAL Id: hal-04930862

<https://hal.science/hal-04930862v1>

Submitted on 5 Feb 2025

HAL is a multi-disciplinary open access archive for the deposit and dissemination of scientific research documents, whether they are published or not. The documents may come from teaching and research institutions in France or abroad, or from public or private research centers.

L'archive ouverte pluridisciplinaire **HAL**, est destinée au dépôt et à la diffusion de documents scientifiques de niveau recherche, publiés ou non, émanant des établissements d'enseignement et de recherche français ou étrangers, des laboratoires publics ou privés.

Development of a Novel Self-locking-at-rest Piezoelectric Inchworm Motor with High Switching Frequency Driving Ability

Sandip Jana, Sofiane Ghenna, Saikat Kumar Shome, Yves Bernard, Arup Kumar Nandi, and Laurent Daniel*

Abstract—In this paper, a novel piezoelectric actuator-based inchworm motor (IM) and its driving mechanism has been proposed for high speed linear application. Three high voltage positive square pulses with appropriate phase sequence amongst them have been applied to the two clamps and one extender of IM to achieve the desired linear translation. Isolated mosfet-based switching (IMSC) and oscillation circuits have been designed to operate the motor at high switching frequencies by dynamically reducing the capacitive reactance of the piezoelectric stack actuators. Consequently, experiments on the characterization of the piezo-actuators have been performed to identify the pre stress on the motor rail. Geometric model of the system has been developed using finite element analysis (FEA) to determine displacement distribution in Clamping Mechanism (CM) and Extending Mechanism (EM) before physically fabricating the motor prototype to verify the driving mechanism. Performance evaluation has been carried out under varying duty cycles, switching frequencies and loads. The motor is observed to achieve a maximum no load speed of 60 mm/sec under the 80-90 volt positive square pulse at a frequency of 3 kHz with a 20% duty cycle. A relatively high electrical driver efficiency of 42% is experimentally achieved which makes the proposed mechatronic system highly suitable for low-size, high torque industrial applications.

Index Terms— Piezoelectric actuator, Modelling, Inchworm, Sensor, Force measurement.

I. INTRODUCTION

To improve performance, safety and cost, there has been a radical shift by the original equipment manufacturers for industrial utilities towards automated and enhanced manual

control of industrial translation applications [1]. There is an increasing tendency towards rising usage of electrical drive remedies as conventional hydraulic and pneumatic controls are often unsuitable for automatic computer controlled operations due to increased system cost and complexity [2]. Besides, assembly and maintenance of conventional systems also requires extra steps along with additional cabling and connectors. Electromagnetic motors offer an alternative solution with several advantages such as compact size, quick response, high power handling capability, high accuracy, in the field of medical technologies, automotive industries, smart robotic system. However, it requires a number of add-on components, including the control and driver circuit for precise position sensing system.

In contrast, smart actuators over traditional hydraulic and pneumatic cylinders are simpler and smaller installation, higher power density, higher accuracy, less maintenance, less noise and clean environment [3-4]. Therefore smart material based actuators like Piezo-Actuator (PA) is a promising candidate for the development of a new type motor which is a relatively innovative concept [5-6]. PA is a crucial transducer used in micro-nano manipulation with promising application in the area of desktop reconfigurable, biomedical, robotics, vibration control, micro displacement technology [7-8]. There are several advantages of piezoelectric actuator, like fast transient response characteristics, small size, high electromechanical coupling efficiency, higher blocking force capability to achieve high resolution positioning accuracy. However, practical usage of PA suffers from different kinds of nonlinear phenomena like hysteresis, creep which seriously affects the position and control accuracy [9-12]. Therefore, accurate modeling of the PA is essential towards compensation of the non-linearities.

In the past few years, the inchworm piezoelectric actuator was studied for many applications. This small size motor can be designed for high force or large step displacement and the travel length only depends on slider dimensions. Other advantages are that it is magnetic field free, high accuracy and stiffness [13-14].

PA was first introduced for the IM by O'Neill in 1980 to increase the actuation travel range [15] wherein two clamping devices are coupled with cups to actuate the clamping devices.

Manuscript received Month xx, 2xxx; revised Month xx, xxx; accepted Month x, xxxx. The authors gratefully acknowledge the funding received from Indo French Center for The Promotion of Advanced Research (IFCPAR/CEFIPRA) for carrying out this work. (Corresponding author: L. Daniel)
S. Jana, S. K. Shome and A. Nandi are with CSIR - Central Mechanical Engineering Research Institute (CSIR-CMERI) Campus, Durgapur 713209, India; Academy of Scientific and Innovative Research (AcSIR), Ghaziabad 201002, India (email:sandip.cmeri19a@acsir.res.in; saikatshome@cmeri.res.in; nandi@cmeri.res.in). S. Ghenna, Y. Bernard and L. Daniel are with Université Paris-Saclay, Centrale Supélec, CNRS, Laboratoire de Génie Electrique et Electronique de Paris, 91192, Gif-sur-Yvette, France; Sorbonne Université, CNRS, Laboratoire de Génie Electrique et Electronique de Paris, 75252, Paris, France and S. Ghenna is also with Univ. Polytechnique Hauts-de-France, CNRS, Univ. Lille, Yncrea, Centrale Lille, UMR 8520 - IEMN-DOAE, F-59313 Valenciennes, France. (e-mail:Sofiane.Ghenna@uphf.fr;yves.bernard@centralesupelec.fr; laurent.daniel@centralesupelec.fr)

The idea of linear motion of the piezoelectric inchworm motor was proposed by Lee et al. using a micro-scale etched electrostatic linear actuator [16-17] which has fast response time and high torque handling capability. System design equations of the IM are proposed using system design tool [18]. The stiffness interaction between the frame and the PA is key to determining the clamping force and how it affects the positioning [19].

The design and implementation of the driver system of IM is a challenging task due to frequency-dependent capacitive effect of the actuator and presence of existing non-linearities like hysteresis, drift and temperature effects. Table 1 gives the performance overview which is suggestive of a limited range of operating frequency of the inchworm motors. PA displacements are usually within a few tens of micrometers. Several linear IMs have been reported to achieve large motions [21, 22, 24, 26, 28, 29, 31], though their speed was limited by low-frequency driving circuits. The maximum thrust force was obtained recently by [34] with a less speed compared to [20]. In order to achieve higher speed, the motor switching frequency, excitation voltage amplitude should be increased. A maximum operating frequency of 1000Hz has been achieved in [20] with a voltage of 124 V. The IM reported [32] has the same operating voltage as [23] with less speed due to operating frequency drop from 800 Hz to 30 Hz. The maximum speed of the IM linear motor was obtained by [35] with reduced frequency and driving voltage compared to [20] as the former was loaded with maximum thrust of 0.6 N in order to achieve the high operating speed. It can thus be observed that though frequency of operation plays a vital role in determining the motor speed, yet the reported literature shows that piezoelectric inchworm motor could be operated upto a maximum frequency of 1000 Hz. The majority of the IM configurations have designed a relatively high volume motor that uses three piezo actuators except in configurations [27, 32, 35] which have even more actuators. In this paper, the IM speed is increased by operating it at higher frequencies through proposed driver circuit along with a smaller motor volume and weight while keeping the number of piezo actuators unchanged.

Additionally, the CMs of the proposed design locks the rotor when unpowered, unlike the configurations described in the literature [20, 23, 25, 27, 30, 33, 34,] that require electrical signals for clamping. The design ensures two blocks on each of the CMs to apply a relatively high blocking force, making the structure self-locking at no power. External electrical excitation is required to de-clamp and unlock the stator from the rotor for a free stroke.

Thus, it is evident that piezo IM motors play an important role due to its simplistic construction and advantages of material properties. However, the reported developments center on low frequency drive and high motor volume. Consequently, the motors generate restricted motion which limits its usage for high speed industrial application.

In our previous work, a design and experimental analysis of a high force piezoelectric linear motor were proposed [36]. Five PAs were used and excited at low frequency (1 Hz) resulting in speed of 2.25 $\mu\text{m/s}$. In the current paper, PA linear motor with similar performances is presented. The rotor is actuated by three PAs instead of five. Moreover, high frequency power

supply (3kHz) is developed and tested.

The specific contributions of this work can be summarized as:

i) Development of mechanical structure and prototype design of the IM, ii) Geometrical modelling of mechanical system and FEA analysis to investigate performance of CMs and EM of the IM, iii) Design and implementation of isolated mosfet based high switching frequency and high voltage driver circuit for long range, high speed linear translation application and its experimental verification, iv) Dynamic modelling of the IM and development of specially designed load end, electrical oscillator circuits, v) Experimental investigation towards performance evaluation of IM with varying the duty cycle, switching frequency and load.

Accordingly the research paper is organized into six sections.

The mechanical structure and design of control mechanism of the inchworm motor are discussed in Section II. FEA analysis of the IM is mechanism and prototype fabrication are presented in section III and IV. The mathematical modelling of the motor is derived in section V. Section VI presents the three phased isolated switching and boost driving mechanism while the experimental result and analysis are presented in section VII. Finally, conclusion is made in section VIII.

II. MECHANICAL STRUCTURE & IM MECHANISM

The proposed mechanical design mainly focuses on high clamping force requirement besides addressing the difficulties associated with the specific integration constraints. The main motive behind this work is to provide a clamping mechanism with full clamping abilities without the activation of the motor i.e self-locking at rest, this is often a required property. The CM generates high blocking force with relatively compact size in terms of dimensions and performances detailed hereafter.

A. Proposed Piezoelectric IM

The new design shown in Fig. 1 includes two CMs (green) and an extender (red) which are fitted with piezoelectric actuators (marked in blue). Screw and nut junction is used to connect the the CMs and EMs while pre-tightening blocks and screws are used as pre-tightening elements. Fixed part of the motor (stator) marked in grey is designed to act as a guide for the moving part as well as to lend a desired blocking force necessary for actuation.

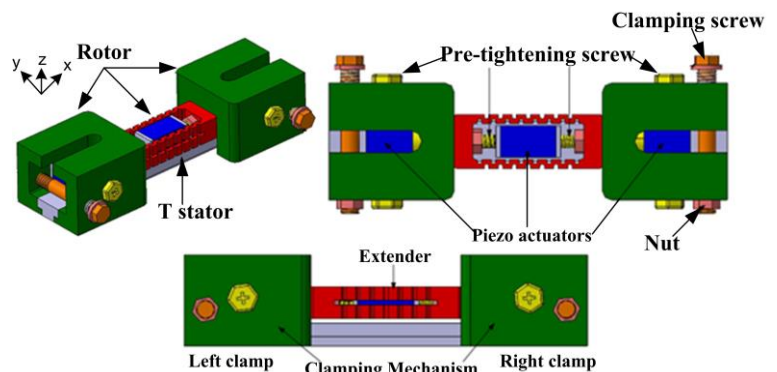


Fig. 1. Proposed piezo based IM design structure with self-locking at rest

TABLE I Performance of reported IMs

References	Driving frequency [Hz]	Speed [mm/sec]	Driving voltage[V]	Maximum Thrust[N]	Number of Piezo Actuators	Volume[cm ³]
1999[20]	1000	6	124	41.5	3	48
2003[21]	15	0.0013	100	-	3	100
2006[22]	-	20	-	10	3	-
2007[23]	800	8.5	200	6	3	-
2011[24]	600	3.60	100	-	3	-
2013[25]	70	2	150	10	3	-
2016[26]	8	0.005	120	43	3	280
2017[27]	110	4	100	10	4	-
2018[28]	180	26.74	10	-	3	44.55
2019[29]	150	1.07	150	70	3	296
2020[30]	50	0.72	120	3.28	3	202.6
2021[31]	3.2	.043	75	-	3	-
2021[32]	30	0.028	200	4.9	2	169
2021[33]	120	1.54	150	1.2	3	432
2022[34]	250	0.043	120	546	3	112
2022[35]	650	44.69	80	0.6	6	116.6

The stator has a T-shape that prevents the rotor from derailing. Screws (marked in orange) along with washer to clamp and spring are used in the design to necessitate a uniform blocking force on the inchworm motor's rotor, seen in Fig 1. Stator of the motor is assumed to be completely rigid with no gap with the rotor. The rotor is blocked on stator through screws and nut. In order to deactivate the CMs, the PAs in the CMs are placed along Y-Axis.

Another interesting property of the designed motor is self locking at rest. Powering up the PAs in the CMs, unlocks it while withdrawal of power, naturally blocks the stator.

A very fine thread pitch have been chosen which has a better technical resistance to loads and allows to have a solid connection but also to obtain a precise adjustment of the restressing force. This force can be controlled by knowing the number of turns. Moreover, the contribution of the PAs is controlled since we have imposed the same prestressing force to balance the contribution of CMs by imposing the same level of applied voltage which can prevent the uneven force between the threads and the pitch gap of the motor. The operating mechanism [37] of the IM comprises a cycle of six steps, as elaborated in Fig. 2.

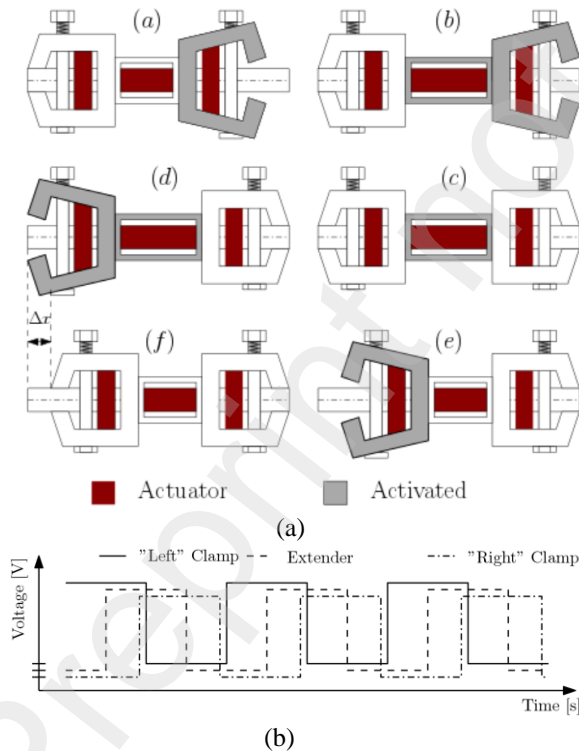


Fig. 2. a) IM operating mechanism comprising six steps. b) Motion generation voltage curve for IM during three cycles.

III. GEOMETRICAL MODELING & FEA ANALYSIS OF THE IM MECHANISM

To compute the performance of the IM for the CM and EM, 3D FEA has been conducted using COMSOL Multiphysics® software.

A. Clamping Mechanisms

The Fig.2 shows that the slider is clamped when the rotor is off. The dimensions shown in fig. 3 have been chosen to obtain a high holding force. Since the displacement of the chosen PA is limited, the PA has been placed as far as possible from the clamping region (the displacement is amplified). Several materials have been modeled to optimize the stiffness regarding dimensions. The selected material is steel (for high friction force rotor/stator) with a density of 7860 kg/m³, elastic modulus of 200 GPa, and poisson ratio of 0.266.

1) Clamp Closure

By the clamping screw, a total contact force (along Y-axis) of 1250N is obtained under applied screw

force of 730 N on both sides. The corresponding clamp displacement distribution along Y-axis in the closing mode is presented in Fig. 3(a).

2) Clamp Aperture

Modeling results indicate that when PA applies a 1600 N force over the clamp, the reaction force on the slider from the clamp is 0. Fig. 3(b) displays the displacement trajectory on applying a force of 1600 N to the PA along Y-axis. At the position of the PA, a displacement of 12 μm ($6 \times 2 \mu\text{m}$) is induced. Hence, a PA with stiffness of $133 \text{ N}\mu\text{m}^{-1}$ is required.

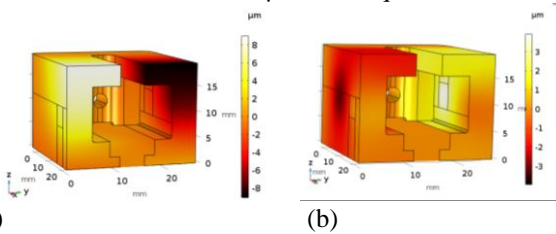


Fig. 3. Clamp displacement distribution along Y-axis a) In the closing mode b) In the opening mode

3) Clamp Closure and Aperture in the Contact Region

The transition between clamp closure and clamp aperture is analyzed. The Von-Mises stress when the clamp is locked and unlocked through the T-rail is shown in Fig.4. (a) and Fig.4.(b) respectively. The absence of stress along the T-rail (contact region) when the clamp is open (Fig.4. (b)) is the evidence of a zero contact force.

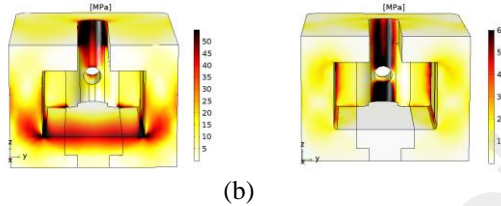


Fig. 4. Von-Mises stress, (a) Clamp closure (b) Clamp aperture

From these two tests, the contact region between stator and rotor has been examined. As can be seen in Fig. 5, when the clamp is closed, the displacement has the same pattern in both clamp and T-rail, because the work applied by the clamp is transmitted to the rail through the contact region. Near the clamping screw (position 17 mm), the rail displacement is $1 \mu\text{m}$ due to the applied force. However, when the clamp is open (a PA force is applied in addition to that of the screw), the distance between rotor and stator increases creating a gap of $2 \mu\text{m}$ in the region of the PA (No contact between stator and rotor).

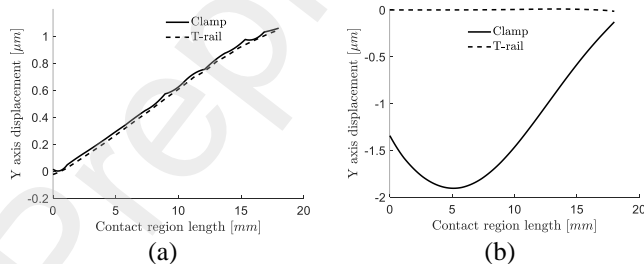


Fig. 5. Displacement at clamp closing (a) and opening (b) in the contact region

B. Extending Mechanisms

It is usual to use PA in a metal case to enhance reliability as a physical interface for linear contact is not obtained between the two Clamping Mechanisms. In the clamp system, the clamp itself was creating the pre-tightening force while, in the EM, we have to design a metal casing which also safeguards the actuators from external hazards and force impacts. The design is centered around the elasticity property of the extending mechanism with its length and breadth dimensions being limited to that of the clamps. The extender, thus, operates as a spring when the PAs are powered on.

C. Extending and Retracting Mode

Modeling results indicates that a displacement of 13 μm is obtained when a 500 N force is applied to the elastic case, Fig.6a. Upon withdrawal of power from the extender, it retracts which is ensured by the fact that the Von-Mises stress is less than the yield stress stainless steel. It has been verified through calculation of Von-Mises stress that the elastic limit was not reached, as seen in Fig.6b. Selection of proper piezo actuator in terms of required force at output, displacement range required, and dimensional restrictions, is hence possible with a knowledge of the inchworm motor stiffness.

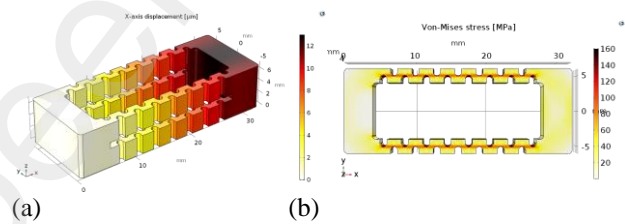


Fig. 6. a) Extender displacement distribution in the extending mode along X-axis (3D view) b) Extender retracting mode along X-axis(3D)

IV. IM PROTOTYPE MANUFACTURING AND ASSEMBLY

A. PAs Characteristic

An intersection of the force displacement graph with the motor structure stiffness is required as the force generated by the PA is linked with reduced elongation. In the experiments, multi-layer NOLIAC piezoelectric stack actuators have been used – NAC 2022 H14 and NAC 2021 H16 for clamps and extender respectively. Specification of PZT stack actuators are given in Table II. Voltage vs displacement characteristics of the piezo-actuators are measured at off-load condition, represents a linear nature, Fig. 7.

TABLE II
SPECIFICATION OF PIEZOELECTRIC STACK USED IN THE IM

Type	Dimensions [mm ³]	Free stroke [μm]	Blocking force [N]	Capacitance [μF]
CM: NAC2022-H14	10x10x14	19.8	4200	2.38
EM: NAC2021-H16	7x7x16	23.1	2060	1.39

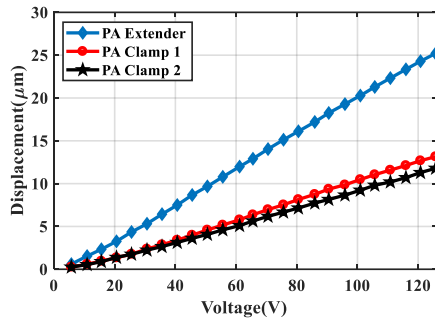


Fig. 7. Forward stroke displacement of free PAs versus applied DC voltage

B. Prototype Assembly

A prototype with dimensions 86 x 26 x 20 mm³ and a weight of 200 g was manufactured. The three individual parts (clamp 1, extender, clamp 2) of the inchworm motor are assembled with the corresponding PA in the clamp and in extender structure as shown in Fig.8.

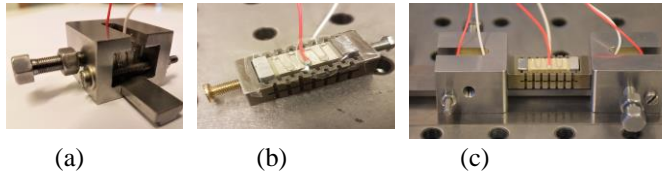


Fig. 8. Inchworm Motor (IM) prototype, (a) Clamping Mechanism (CM) with PA, (b) Extender Mechanism (EM) and (c) fabrication of constituent parts

C. Pre-stress Force Measurement of PAs using Force Sensor

The PAs used in the development of the IM need to be calibrated for accurate system response. Pre-stress forces have been applied by the Compression Digital Hand Tester (CHDT) to the PA and the corresponding analog voltage signals have been observed in DSO, as measured by the force sensor, seen in Fig. 9 (a). Pre-stress force is increased from 80 N to 200 N and corresponding change of voltage are increased from δ_5 to δ_1 ($\delta_1 > \delta_2 > \delta_3 > \delta_4 > \delta_5$). It is seen that the maximum pre stress force 200 N can be measured at change of voltage δ_1 . The force vs voltage plot of the experimental pre-stress measurement data (Fig. 9 (b)) fits with linear characteristics suggesting the dependency of voltage on force of the PAs is linear.

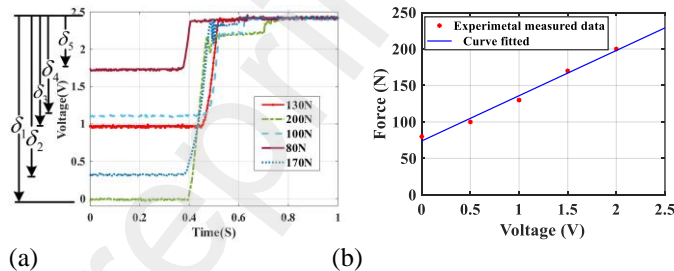


Fig. 9. a) Prestressing force measurement plot of PA for IM b) force vs voltage relationship of PA with linear curve fitting

V. MATHEMATICAL MODELING OF THE INCHWORM MOTOR

In this section, dynamic modelling of piezo-based IM is developed in MATLAB Simulink platform to ensure that

positive driving pulses traverse across the piezo-actuators of the motor. The normal applied force is directly proportional to the applied voltage of the motor. Resultant linear displacement by the motor is achieved due to movement of extender fitted between the two clamps and the rotor. Frictional force of clamp 1 between guide wall and clamping chamber is represented as equation 5 and 6, where, \dot{x}_{c1} and \dot{x}_{c2} are the velocity of left and right clamps with V_{c1} , V_{c2} and V_e being the applied voltage on the two clamps and extender. A small speed v_0 ($v_0 > 0$) is defined to represent the situation at which the body can be considered stationary (e.g. $\dot{x}_{c1}, \dot{x}_{c2} < v_0$). The coefficient 'a' of equation (5) is constant which is proportional to the friction coefficient ' μ ' and can be calculated by piezoceramic one dimensional equation [38]

The sign and saturation function can be defined as

$$\text{sign}(x) = \begin{cases} 1, & x > 0 \\ 0, & x = 0 \\ -1 & x < 0 \end{cases}, \text{sat}(x) = \begin{cases} 1, & x > 1 \\ 0, & -1 \leq x \leq 1 \\ -1 & x < -1 \end{cases}$$

Where F_0 represents either F_{0c1} and F_{0c2} which are the two forces acting on clamp 1 and clamp 2 of the inchworm motor. Two clamping forces of the clamps are presented as

$$F_{0c1}(X, \dot{X}, V_e) = -F_p(V_e) + k_1(x_e - x_{c1}) + C_{c1}(\dot{x}_e - \dot{x}_{c1}) \quad (1)$$

$$F_{0c2}(X, \dot{X}, V_e) = -F_p(V_e) + k_2(x_e - x_{c2}) + C_{c2}(\dot{x}_e - \dot{x}_{c2}) \quad (2)$$

Where, x represents position vector represented as

$$x = \begin{Bmatrix} x_{c1} \\ x_e \\ x_{c2} \end{Bmatrix}^T \quad x_{c1} = \text{displacement of clamp1}, x_e = \text{displacement of the middle actuator or extender}, x_{c2} = \text{displacement of the clamp 2 of the motor}, V_e = \text{voltage applied to the extender piezo stack}, F_p \text{ represents as a pushing force exerted by the piezoelectric stack actuator on the mechanical structure.}$$

The dynamic model of proposed piezoelectric IM represented in Fig. 10 has been mathematically modelled as

$$M\ddot{X} + C\dot{X} + KX = F_{fr} + F_p \quad (3)$$

where, F_{fr} represents the frictional force and longitudinal piezo stacks exert a pushing force on the motor frame of the motor which is indicated by F_p . The system can be designed in non-linear state space form as

$$\dot{x} = [A]x + g(u, x), \quad y = [C]x \quad (4)$$

where, $[A]$ and $[C]$ are input, output matrix of the system, 'y' is displacement of the middle actuator (extender) and 'x', 'u' are the system state, input vector, accordingly and defining them as follows:

$$x = \{x_{c1} \quad x_e \quad x_{c2} \quad \dot{x}_{c1} \quad \dot{x}_e \quad \dot{x}_{c2}\}^T \quad u = \{V_{c1} \quad V_e \quad V_{c2}\}^T$$

$$g(u, x) = \begin{Bmatrix} 0 \\ 0 \\ 0 \\ F_{fr1}(V_{c1}, \dot{x}_{c1}) - V_e d \\ 0 \\ F_{fr2}(V_{c2}, \dot{x}_{c2}) + V_e d \end{Bmatrix}^T, \quad C = \{0 \quad 1 \quad 0 \quad 0 \quad 0 \quad 0\}$$

A single PA can be modelled as second order spring mass damper system [39]. As IM is designed using three piezoelectric stack actuators, the overall system can be represented as a second order mass spring damper system with

the two clamps and one extender of the motor being represented through equation (6), (7), (8) respectively.

$$F_{frc1}(V_{c1}, \dot{x}_{c1}) = \begin{cases} -aV_{c1} \text{sign}(\dot{x}_{c1}), & |\dot{x}_{c1}| \geq v_0 \\ -F_0 \text{sat}(\frac{aV_{c1}}{F_0}), & |\dot{x}_{c1}| < v_0 \end{cases}, F_{frc2}(V_{c2}, \dot{x}_{c2}) = \begin{cases} -aV_{c2} \text{sign}(\dot{x}_{c2}), & |\dot{x}_{c2}| \geq v_0 \\ -F_0 \text{sat}(\frac{aV_{c2}}{F_0}), & |\dot{x}_{c2}| < v_0 \end{cases} \quad (5)$$

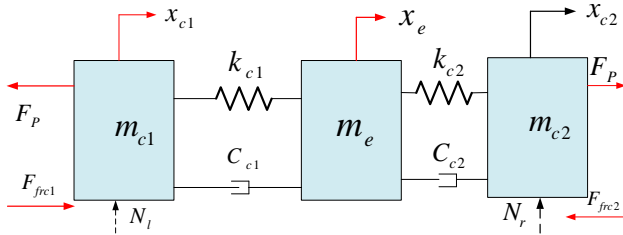


Fig. 10. Dynamic model of the inchworm motor

Dynamic equation for clamp 1 system is

$$\ddot{x}_{c1} = -\frac{C_{c1}}{m_{c1}} \dot{x}_{c1} + \frac{C_{c1}}{m_{c1}} \dot{x}_e - \frac{k_{c1}}{m_{c1}} x_{c1} + \frac{k_{c1}}{m_{c1}} x_e - \frac{K}{m_{c1}} x_{c1} + \frac{K}{m_{c1}} x_e - \frac{V_e d}{m_{c1}} + \frac{F_{frc1}(V_{c1}, \dot{x}_{c1})}{m_{c1}} \quad (6)$$

Dynamic equation for extender system is

$$\ddot{x}_e = -(\frac{C_{c1}}{m_e} + \frac{C_{c2}}{m_e}) \dot{x}_e + \frac{C_{c1}}{m_e} \dot{x}_{c1} + \frac{C_{c2}}{m_e} \dot{x}_{c2} + \frac{k_{c1}}{m_e} x_{c1} + \frac{k_{c2}}{m_e} x_{c2} - (\frac{k_{c2}}{m_e} + \frac{k_{c1}}{m_e}) x_e \quad (7)$$

Dynamic equation for clamp 2 system is

$$\ddot{x}_{c2} = -\frac{C_{c2}}{m_{c2}} \dot{x}_{c2} + \frac{C_{c2}}{m_{c2}} \dot{x}_e - (\frac{K}{m_{c2}} + \frac{k_{c2}}{m_{c2}}) x_{c2} + \frac{K}{m_{c2}} x_{c1} + \frac{k_{c2}}{m_{c2}} x_e + \frac{V_e d}{m_{c2}} + \frac{F_{frc2}(V_{c2}, \dot{x}_{c2})}{m_{c2}} \quad (8)$$

where, C_{c1} =damping coefficient of clamp 1, C_{c2} =damping coefficient of clamp 2, k_{c1} =stiffness of the clamp 1, k_{c2} =stiffness of the clamp 2, K = stiffness of longitudinal piezo stacks, m_{c1} =mass of the clamp 1, m_e = mass of the extender, m_{c2} = mass of the clamp 2. Dynamic equation (6), (7) and (8) are used to design the proposed inchworm motor.

VI. SYSTEM DESCRIPTION

The block diagram of proposed electrical driving system is shown in Fig. 11 where a high switching isolated driver circuit for piezoelectric actuator based IM is developed which includes three step-up converters and three mosfet based switching circuits for the two clamps and one extender. Three isolated 24 Volts battery sources are used as an input power supply to operate the whole system because motor has three phases and each of phase should be isolated to each other. Three DC-DC step-up high wattage non isolated converters have been developed to step up the voltage from 24 Volts to 120 Volts DC.

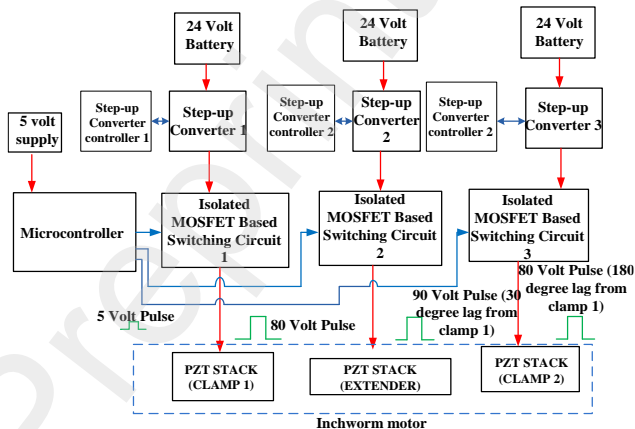


Fig. 11. Block diagram of the proposed electrical driving system of IM

The integrated controller of the step up converter can control the magnitude of the driving voltage. Isolated mosfet based switching circuits (IMSC) generates three isolated phase shifted synchronized pulse for two clamps (80 Volts magnitude) and one extender (90 Volts magnitude) for the IM besides isolating the microcontroller control pulses from the driver unit.

A. Design of Equivalent Oscillator Circuit at Load End to Actuate Capacitive Piezo Element at High Frequency

An equivalent oscillator circuit is designed across each PA of the IM to operate the motor around resonant frequency (derived in eqn 9) to achieve maximum output power and efficiency. A designed inductor 271 μ H for each clamp and 318 μ H for the extender are connected in parallel across the piezo-actuator to make the overall circuit resistive in nature at resonance and eliminate reactive power. An external capacitor (C_e) is connected in series to the capacitive clamp PA ($C_p=2.38 \mu$ F) to reduce the equivalent capacitance value as well as to increase the operating frequency of the clamp circuit as shown in Fig. 12 (a).

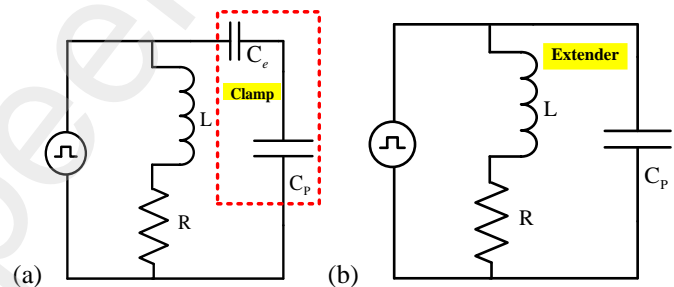


Fig. 12. Equivalent oscillator circuit diagram for operation of the IM connected at load end of each stack actuator a) clamp b) extender

$$f = \frac{1}{2\pi} \sqrt{\frac{1}{LC_p} - \frac{R^2}{L^2}} \quad (9)$$

The inductor value of the circuit is set as per

$$L = \frac{1 \pm \sqrt{(1 - 4\omega^2 C_p^2 R^2)}}{2\omega^2 C_p} \quad (10)$$

Accordingly, the frequency range should be $4\omega^2 C_p^2 R^2 < 1$

$$\text{Therefore, } f < \frac{1}{4\pi C_p R} \quad (11)$$

With an equivalent capacitance of the clamp circuit as 1.19 μ F and assuming the resistance to be 15 Ohms, the operating frequency range is found to be $f < 4.46$ kHz for NAC 2022 H14 two PZT stacks and $f < 3.818$ kHz for NAC2021 H16 PZT stack for the extender.

B. Circuit Diagram of High Switching Driving Unit

Digital micro-controller dsPIC30F4011 is used to generate three phase synchronized 5 Volts magnitude control pulses to actuate the inchworm motor in-line with the operating principle shown in Fig. 13. The three control pulses have been isolated from driver circuit through opto-coupler based gate driver. The two clamps are applied with PWM pulses with 180 degrees phase shift while extender is subjected to a 30 degree phase shift. The switching frequency varies between 50-3000

Hz, operating at duty cycle of 20% and 30%. During the operation of each IMSC, 80-90 Volts magnitude positive square pulse is generated between the positive terminal of the output of each step up converter and drain terminal of the mosfet, to drive the IM.

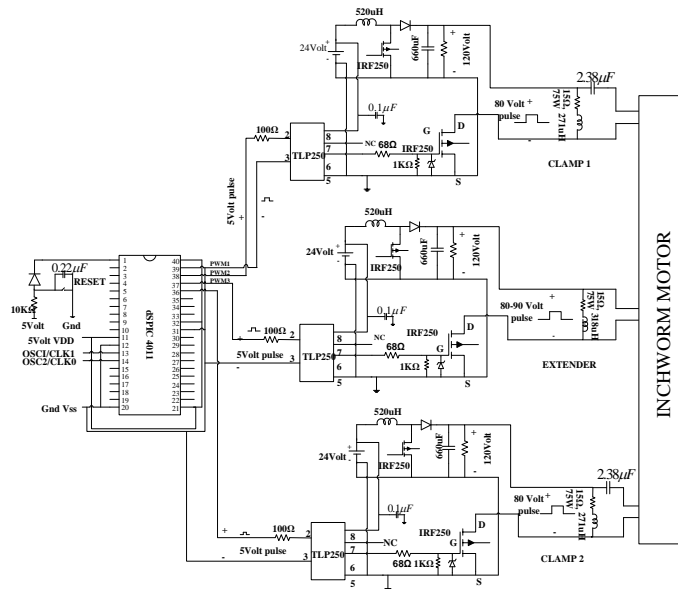


Fig. 13. Circuit diagram of driver unit for actuation of IM

VII. EXPERIMENTAL RESULT AND ANALYSIS

The experimental test bench set up of the proposed system is illustrated in Fig. 14. An IMSC inchworm motor driver circuit has been developed to generate appropriate driving signal from respective control pulses to actuate the motor. An opto NCDT laser displacement sensor ILD2300 (Resolution of $0.8 \mu\text{m}$ at 20 kHz frequency) is interfaced to the motor for measuring the displacement at higher frequencies. The laser displacement sensor is connected to the C-Box and ILD2300 sensor tool software is accessed through the ethernet port of the C-box. As discussed in section IV, the experimental setup considers blocking force as 5 N, and loads are attached to the motor's rotor through a pulley arrangement system for testing. In this experimental work, the clamping force and maximum driving force are significantly different from the theoretical analysis (section III) and maximum performance of the motor has not been tested due to limitation of switching frequency and applied driving voltage level of the driving circuit.

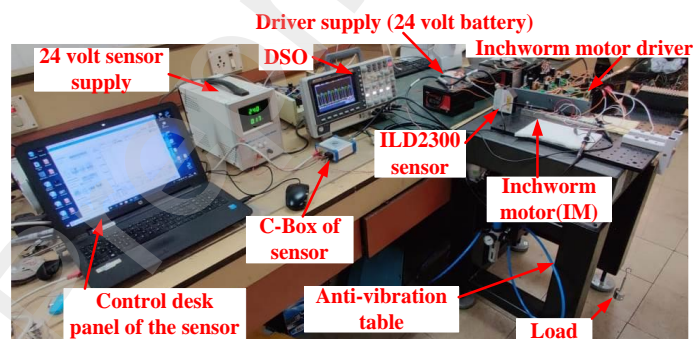


Fig. 14. Experimental test bench set-up for the proposed system

A. IM Step Displacement curve at Lower Operating Frequency without Loading Effect

The step displacement of the inchworm motor (11 cycles) and zoom viewed of two cycles have been shown in Fig. 15, wherein Ch_3 voltage have been used to operate the actuators in left clamping mechanisms, resulting in a axial displacement which releases the clamp from stator. Consequently, Ch_2 voltage is used to excite the extender, and the corresponding displacement is recorded. The left clamping mechanism gets released and right clamping mechanism (Ch_1) gets activated during the later half of Ch_3 . Retraction of the left clamp and its return to previous dimension can be related to reduce observed displacement in DSO. As the displacement is recorded on the left CM which is closed, a fixed displacement is obtained in this interval.

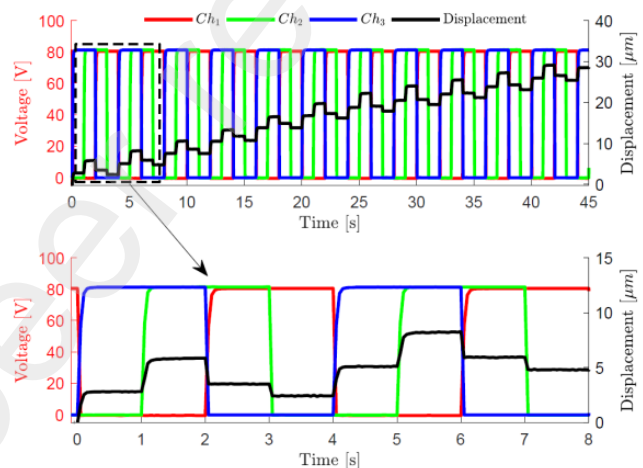


Fig.15. Step displacement curve of 11 cycles at 0.25 Hz frequency

B. IM Tested at 1 kHz Switching Frequency without Loading Effect

The IM has been tested at high switching frequency of 1 kHz with 30% on-time phase synchronized driving pulses (Fig.16), the corresponding displacement and speed have been measured by laser displacement sensor to be 3.76 mm and 5.88 mm/sec respectively. Displacement is observed to increase linearly when motor moves in forward direction as shown in Fig.17 (a), (b).

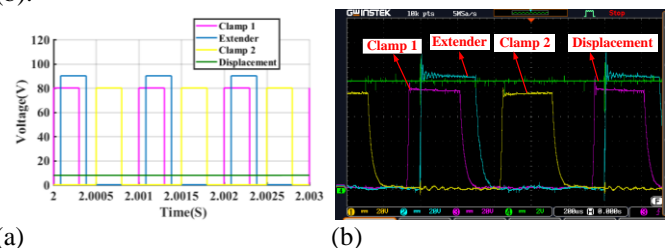


Fig. 16. a) Simulated from model: displacement (in term of voltage) waveform shown in green; positive driving voltage (1 kHz) waveform for forward linear motion of the IM : violet and yellow are two clamp signals (80 V), blue is extender signal (90 V) b) experimental

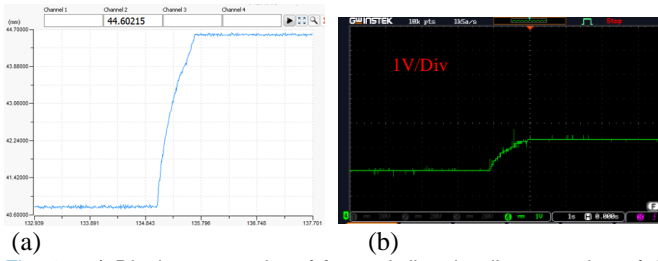


Fig. 17. a) Displacement plot of forward direction linear motion of the proposed IM b) corresponding linear variation of displacement in terms of voltage observed in DSO

C. Performance Characteristics of IM with Varying Duty Cycle and Switching Frequency at No Load

Performance of the IM has been tested at different operating frequencies and duty cycles. Duty cycle is the ratio of linear actuators running vs resting time typically varies range of 10-70% and mostly depending on load. Increasing the speed and load on PA can lead to overheating, which reduces the actuator's life expectancy. Therefore, to increase load capacity and speed, driving pulse duty cycle has been decreased.

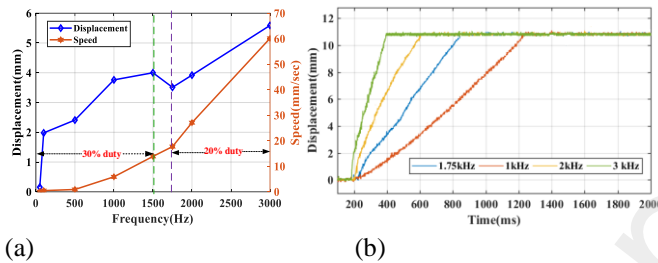


Fig. 18. a) Experimental displacement and speed measurement plot of IM by varying operating frequency and duty cycle b) Experimental operating characteristics of IM at different frequency

Displacement of the IM has been measured experimentally by laser displacement sensor. The driving frequency of the motor is linearly varied upto 1500 Hz at 30 % duty cycle, resulting a speed of 13.88 mm/sec, as shown in Fig. 18. (a) The motor is further operated from 1750 Hz to 3000 Hz at 20 % duty cycle and in this case the speed variation of the inchworm motor is seen to be better than the operation at 30% duty. Maximum speed of 60.15 mm/sec is achieved at 3 kHz frequency with 20 % duty cycle. Frequencies of the driving signal of the inchworm motor are varied from 1 kHz to 3 kHz at 20 % duty to realize the desired motion, Fig. 18. (b). It is seen that when the motor is operated at higher frequency, it takes lesser time to bring about the desired motion compared to lower frequency operation. Fig. 18(b) shows a slight fluctuation which may be caused by vibration of the motor due to its high switching frequency or rough contact between the stator and rotor.

D. Displacement and Speed Characteristics with Variation of Load

The motor has been experimented under different loading effect using 1.5 kHz 30% duty cycle control pulse. Displacement and speed linearly decreases due to increase in load as reflected in Fig. 19 (a). Speed of the motor decreases from 0.87 mm/sec to 0.45 mm/sec with an increase of load from 2 N to 4 N. Displacement and speed characteristics of

inchworm motor are shown in Fig. 19 (b) when operated at 3 kHz frequency and 20% duty ratio.

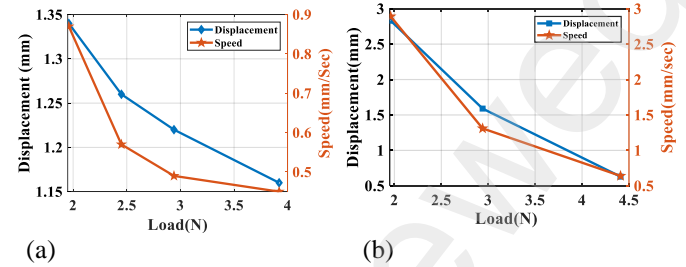


Fig. 19. a) Experimental displacement and speed characteristics of IM due to load variation for 1.5 kHz 30% duty b) Experimental displacement and speed characteristics of IM due to load variation for 3 kHz 20% duty.

At load of 4.41 N, the speed of the motor is measured to be 0.64 mm/sec. Thus, the loading capability is seen to improve if the motor is operated at higher switching frequency and lower duty ratio. The inchworm motor is then operated with different loading capacities at different frequencies against a 2 N load attached the IM through a cable and pulley setup as seen in Fig. 20 (a). Motor is operated at 80-90 Volts and tested at different frequencies mentioned in fig. The speed vs frequency bar diagram of the IM is shown in Fig. 20 (b), where the motor driven at 3 kHz can pull a load of 2 N at a speed of 2.89 mm/sec. The motor speed increases with increasing frequency regardless of whether it is loaded or not. However, in case of loaded condition, the motor speed decreases in comparison to unloaded condition.

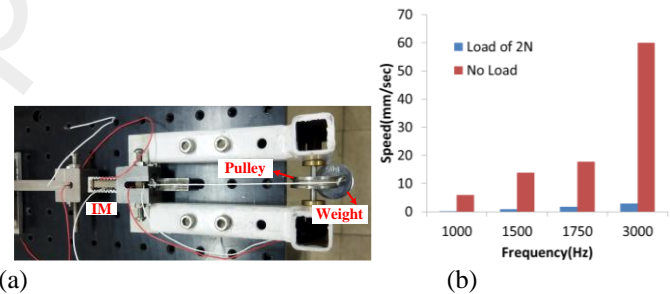


Fig. 20. Impact on speed of the motor with variation of frequency with and without load

E. Efficiency Calculation

Measurement was done by calculating the mechanical work during given period of time, corresponding to its power consumed, calculated by measuring the voltage and current of each channel as shown in Table III. Efficiency (electrical input power to mechanical output power) of IM is calculated 29% (operating voltage 80-90 Volts and frequency- 3 kHz) which is better than 17% reported for electrostatic inchworm motor operated at 110 V and 600 Hz frequency [24]

TABLE III
EFFICIENCY CALCULATION OF ELECTRICAL DRIVER AND IM

Measurement of efficiency	Output power of electrical driver		Input power of electrical driver		Efficiency (%)
	CM1 [watt]	EM [watt]	CM2 [watt]	EM [watt]	
Electrical driver efficiency while the IM is operated at no load	44.73	7.98	107	16.2	42
Mechanical efficiency of IM with driving load of 0.98N	31.7	4.34	104	17.21	29

Experimental multi-parameter comparison of the developed IM has been carried out with similar works reported earlier at low operating frequency [24, 35, 40-45] as shown in Table IV. The present design can actuate at a wide range of operating frequency, upto 3 kHz which is sixty times of IM mentioned in [43]. Consequently our design attains a maximum speed of 60 mm/sec which makes it a promising candidate for high speed, millimeter range longitudinal displacement.

VIII. CONCLUSION

In this research, piezo-based linear inchworm motor is proposed, designed and tested which achieves millimeter range

TABLE IV
COMPARATIVE ANALYSIS OF THE PROPOSED IM WITH PREVIOUS REPORTED WORK

Parameters	Motor [40]	Motor [41]	Motor[42]	Motor [43]	Motor [44]	Motor [35]	Motor [24]	Motor [45]	Proposed IM
Driving voltage [V]	100	100	100	120	100	80	110	80	80-90
Operating frequency [Hz]	200	500	415	50	320	650	600	160	50- 3000
Maximum speed [mm/sec]	5.4	5.96	18.84	0.72	20	44.69	3.6	8.2	60
Maximum thrust force/Load [N]	8.8	3	3.52	N/A	150	0.6	0.0007	0.5	4.41
No of piezo actuators	4	NA	NA	3	3	6	4	3	3
Efficiency [%]	NA	NA	2.07	Low	NA	Low	17	18.5	29
Travel range[mm]	20	0.12	0.42	11	NA	4.3	0.06	NA	80
Self-locking at rest [Y/N]	Y	N	N	N	N	N	N	Y	Y
Type of Piezo Motor	Piezo-IM	Stick-slip	Stick-slip	Inchworm	Inchworm	Inchworm	Inchworm	Inchworm	Inchworm
Volume [cm ³]	658.38	NA	NA	202.5	100.98	116.6	NA	262.5	44.72

APPENDIX

The simulink model parameters of the inchworm motor are considered as: $C_{c1}=1.56$ kNs/m; $k_{c1}=25*\exp(6)$ N/m; $K=1000$ N/m; $C_{c2}=1.56$ kNs/m; $k_{c2}=25*\exp(6)$ N/m; $d=443*\exp(-12)$; $m_{c1}=0.44$ kg; $m_c=0.24$ kg; $m_{c2}=0.44$ kg; $F_{pmax}=1250$ N and maximum clamping force is considered as 5 N and frictional coefficient(μ)=0.31.

Funding This work received funding from the IFCPAR (Indo-French Centre for the Promotion of Advanced Research) under the grant number IFC/7123. It also received direct support from the company Faurecia.

Data availability No datasets were generated or analysed during the current study.

Declarations

Conflict of interest The authors declare no conflict of interest.

REFERENCES

- M. Shafik, E. M. Shehab & H.S. Abdalla, "A linear piezo-electric ultrasonic motor using a single flexural vibrating bar for electro-discharge system industrial applications". *Int J Adv Manuf Technol*,45, doi.org/10.1007/s00170-009-1955-5, 287 (2009).
- M. Tai, P. Hingwe and M. Tomizuka, "Modeling and control of steering system of heavy vehicles for automated highway systems," in *IEEE/ASME Transactions on Mechatronics*, vol. 9, doi: 10.1109/Tmech.2004.839047, no. 4, pp. 609-618, Dec. 2004.
- R. Taleb, L. Seddiki, K. Guelton and H. Akgad, "Merging fuzzy observer-based state estimation and database classification for fault detection and diagnosis of an actuated seat," *2017 IEEE International Conference on Fuzzy Systems*.
- A. Zyner, S. Worrall, and E. Nebot, "A recurrent neural network solution for predicting driver intention at unsignalized intersections," *IEEE Robot. Autom. Lett.*, vol. 3, no. 3, pp. 1759-1764, Jul. 2018.
- S. Jana, SK. Shome & A. Mukherjee, "Polynomial-based Stability Analysis of Modified IMC-PID Controller for Piezoelectric Actuator System in Time Delay Environment", *IETE Journal of Research*, DOI: 10.1080/03772063.2021.1987996,2021
- S. Ghenna, F. Giraud, C. Giraud-Audine and M. Amberg, "Vector Control of Piezoelectric Transducers and Ultrasonic Actuators," in *IEEE Transactions on Industrial Electronics*, vol. 65 doi: 10.1109/TIE.2017.2784350., no. 6, pp. 4880-4888, June 2018,
- D. Guo, W. S. Nagel, G. M. Clayton and K. K. Leang, "Spatial-Temporal Trajectory Redesign for Dual-Stage Nanopositioning Systems With Application in AFM," in *IEEE/ASME Transactions on Mechatronics*, vol. 25, doi: 10.1109/Tmech.2020.2971755, no. 2, pp. 558-569, April 2020.
- X. Liu et al., "Vortex-Driven Rotation for Three-Dimensional Imaging Under Microscopy," in *IEEE Transactions on Nanotechnology*, vol. 17, doi: 10.1109/Tnano.2018.2811958, pp. 688-691, July 2018.

displacement with better efficiency. The paper focuses on the modeling and FEA analysis of inchworm along with high clamping force requirement with specific integration constraints. Measurement of the pre-stress has been carried out to improve the mechanical output ability. The proposed IM prototype could simultaneously achieve high frequency, high voltage operation by mosfet-based control and electrical capacitance balancing circuitry designed across piezo-actuators. Performance characteristics have then been experimentally evaluated with different operating parameters such as frequency, duty cycle and loading effect. The motor can be operated at a maximum frequency of 3 kHz with 20 % duty cycle and achieves maximum no-load speed of 60 mm/sec. The electrical efficiency of the driver circuit and the mechanical efficiency of the inchworm motor have been calculated to be 42% and 29% respectively. The proposed system can be used for applications requiring high speed, large force and high torque like actuation of aeroplane pilot seats, automobile seats.

- [9] Y. Qin, Y. Tian, D. Zhang, B. Shirinzadeh and S. Fatikow, "A Novel Direct Inverse Modelling Approach for Hysteresis Compensation of Piezoelectric Actuator in Feedforward Applications" *IEEE/ASME Transactions on Mechatronics* 18 981-989, 2013.
- [10] M. Rakotondrabe, "Bouc-Wen Modelling and Inverse Multiplicative Structure to Compensate Hysteresis Nonlinearity in Piezoelectric Actuators" *IEEE Transactions on Automation Science & Engineering* 8 428-431, 2011.
- [11] S. Shome, S. Jana, A. Mukherjee, P. Bhattacharjee, "Design of Adaptive Voltage Dither Control Framework Based on Spectral Analysis for Nonlinear Piezoelectric Actuator". *J Control Autom Electr Syst*, 30, doi.org/10.1007/s40313-019-00506-6 954-969, 2019.
- [12] R. U. Chang-Hai, Z.H. Wang, L. G. Chen and L. N. Sun, "A Hysteresis Control Model of Piezoelectric Actuator Based on Microscopic Polarization Mechanisms" *Control Engineering of China* 17, 2010
- [13] G.L. Locher, Micrometric Linear Actuator, Patent #3,296,467, 1967.
- [14] X. Tian, Q. Quan, L. Wang, and Q. Su, "An Inchworm Type Piezoelectric Actuator Working in Resonant State," in *IEEE Access*, vol.6, pp. 18975-18983, 2018
- [15] O. Neill et al. "Electromotive actuator" U.S. patent number 4,219,755, August 26, 1980.
- [16] S. Lee and M. Esashi, "Design of the Electrostatic Linear Micro actuator Based on the Inchworm Motion", *Mechatronics*, Vol. 5, No. 8, pp. 963-972, 1995.
- [17] M. Vaughan, D. J. Leo, "Integrated Piezoelectric Linear Motor For Vehicle Applications" *ASME International Adaptive Structures and Materials Systems Symposium* November 17-22, 2002.
- [18] P.E. Tenzer, and R. B. Mrad, "A systematic procedure for the design of piezoelectric inchworm precision positioners," in *IEEE/ASME Transactions on Mechatronics*, vol. 9, no. 2, pp. 427-435, June 2004.
- [19] S. Canfield, B. Edinger, M. Frecker, and G. Koopmann, "Design of Piezoelectric Inchworm Actuator and Compliant End-Effectors for Minimally Invasive Surgery", *SPIE Proceedings*, Vol. 3668, pp. 835-843, 1999.
- [20] Galante T. et al. Design, modeling, and performance of a high force piezoelectric Inchworm motor. *J Intell Mater Syst Struct* 1999;10(12):962-72. <http://dx.doi.org/10.1106/21LN-RUY-35CH-C1FD>
- [21] Cho N, Jang W. The design and characterization of a Piezo-driven Inch-worm linear motor with a reduction-lever mechanism. *JSME Int J Ser C* 2004;47(3):803-11. <http://dx.doi.org/10.1299/jsmec.47.803>.
- [22] Moon C, et al. A new fast Inchworm type actuator with the robust I/Q heterodyne interferometer feedback. *Mechatronics* 2006;16(2):105-110. doi.org/10.1016/j.mechatronics.2005.10.003.
- [23] Salisbury SP, Mrad RB, Waechter DF, Prasad SE. Characterization of a Piezoworm stage. In: 2007 IEEE/ASME international conference on advanced intelligent mechatronics. 2007, p. 1-5. <http://dx.doi.org/10.1109/AIM.2007.4412444>
- [24] Penskiy, AP. Gerratt, and S. Bergbreiter "Efficient electrostatic inchworm motors with simple control and high force density," 16th International Solid-State Sensors, Actuators and Microsystems Conference 2011, doi: 10.1109/Transducers.2011.5969660, 2011, pp. 2438-2441
- [25] Ma L, Jiang C, Xiao J, Wang K, Xie W, Liu B. A piezoelectric Inchworm actuator based on the principle of flexible amplification. In: 2013 international conference on manipulation, manufacturing and measurement on the nanoscale. 2013, p. 201-6. <http://dx.doi.org/10.1109/3M-NANO.2013.6737414>.
- [26] S. Wang, W. Rong, L. Wang, and L. Sun, "Design, analysis and experimental performance of a stepping type piezoelectric linear actuator based on compliant foot driving" *Smart Materials and Structures* 25 115003
- [27] Sun M, et al. Research on a novel non-resonant piezoelectric linear motor with lever amplification mechanism. *Sensors Actuators A* 2017;261(Supplement C):302-10. <http://dx.doi.org/10.1016/j.sna.2017.04.030>
- [28] S. Siyan, S. Shao, M. Xu, Y. Shao, Z. Tian, B. Feng, "Piezoelectric inchworm rotary actuator with high driving torque and self-locking ability", *Sensors and Actuators A: Physical*, Volume 282, 2018, Pages 174-182.
- [29] Tahmasebipour M, Sangchap M. A novel high performance integrated two-axis Inchworm piezoelectric motor. *Smart Mater Struct* 2019;29(1):015034. <http://dx.doi.org/10.1088/1361-665X/ab545e>.
- [30] Dong H, Li T, Wang Z, Ning Y. Design and experiment of a piezoelectric actuator based on Inchworm working principle. *Sensors Actuators A* 2020;306:111950. <http://dx.doi.org/10.1016/j.sna.2020.111950>
- [31] R. Wang, Y. Hu, D. Shen, J. Ma, J. Li and J. Wen, "A Novel Piezoelectric Inchworm Actuator Driven by One Channel Direct Current Signal," in *IEEE Transactions on Industrial Electronics*, vol. 68, doi: 10.1109/TIE.2020.2975493, no. 3, pp. 2015-2023, March 2021.
- [32] Cai J, Chen F, Lining S, Dong W. Design of a linear walking stage based on two types of piezoelectric actuators. *Sensors Actuators A* 2021;332:112067
- [33] Tian Yanling, Huo Zhichen, Wang Fujun, et al. A novel friction-actuated 2-DOF high precision positioning stage with hybrid decoupling structure. *Mech Mach Theory* 2022;167:104511.
- [34] Shubao S, Siyang S, Yan S, Minglong X. Long-range piezoelectric actuator with large load capacity using Inchworm and stick-slip driving principles. *Precis Eng* 2022;75:167-79.
- [35] J. Ling, L. Chen, Z. Feng, Y. Zhu, "Development and test of a high speed pusher-type inchworm piezoelectric actuator with asymmetric driving and clamping configuration", *Mechanism and Machine Theory*, Volume 176, 2022, 104997, ISSN 0094-114X, <https://doi.org/10.1016/j.mechmachtheory.2022.104997>
- [36] S. Ghenna, Y. Bernard, and L. Daniel, "Design and experimental analysis of a high force piezoelectric linear motor," *Mechatronics*, vol. 89, p. 102928, Feb. 2023, doi: 10.1016/j.mechatronics.2022.102928.
- [37] S.K. Shome, S. Jana, P. Bhattacharjee, "On learning-based approaches in power electronics engineering curriculum: A high switching inchworm motor drive case study," - *Computer Applications in Engineering Education*, Volume 28, doi.org/10.1002/cae.22258 Issue 4 2020
- [38] K. Uchino 1997 Piezoelectric Actuators and Ultrasonic Motors. Dordrecht: *Kluwer Academic publishers*.
- [39] Q. Xu, Y. Li, "Dahl model-based hysteresis compensation and precise positioning control of an XY parallel micromanipulator with piezoelectric actuation" *Journal of Dynamic System, Measurement and Control* 2010, doi: 10.1115/1.400171,132 (4): 41011.
- [40] T. Mohammad and S. P. Salisbury, "Design and assessment Of A Z-Axis precision positioning stage with centimeter range based On A piezoworm motor," *IEEE-ASME Trans. Mechatronics*, vol. 20, no. 5, pp. 2021-2030,
- [41] T. H. Cheng, M. He, H. Y. Li, X. H. Lu, H. W. Zhao, and H. B. Gao, "A novel trapezoid-type stick-slip piezoelectric linear actuator using right circular flexure hinge mechanism," *IEEE Trans. Ind. Electron.*, vol. 64, no. 7, pp. 5545-5552, Jul. 2017.
- [42] X. Zhang, Y. Yu, Q. Gao, G. Qiao, Z. Li, X. Lu, T. Cheng, A stick-slip linear piezoelectric actuator with mode conversion flexible hinge driven by symmetrical waveform, *Smart Mater. Struct.* 29 (5) (2020) 055035.
- [43] H. Dong, T. Li, Z. Wang, Y. Ning, Design and experiment of a piezoelectric actuator based on inchworm working principle, *Sensors Actuators A* (2020) 111950
- [44] P. E. Tenzer and R. B. Mrad, "A systematic procedure for the design of piezoelectric inchworm precision positioners," in *IEEE/ASME Transactions on Mechatronics*, vol. 9, doi: 10.1109/Tmech.2004.828627, no. 2, pp. 427-435, June 2004.
- [45] L. Guo He, Q. Zhang, C. Liang Pan, B. Ju, Z. H. Feng, "Piezoelectric motor based on synchronized switching control", *Sensors and Actuators A: Physical*, Volume 197, 2013, Pages 53-61, ISSN 0924-4247, <https://doi.org/10.1016/j.sna.2013.03.033>.



converters, piezo electric actuator system and motor control.



France. His research interests include design, modeling and control of smart materials based actuators.



piezoelectric devices. Since 2012, he is professor with a research topic on piezo motors.



Laurent Daniel received Ph.D. degree from Ecole Normale Supérieure de Cachan, Cachan, France, in 2003 and Habilitation degree in Physics from the Université Paris-Sud, Orsay, France, in 2011. Since 2015, he has been a Full Professor with Centrale Supélec, Université Paris-Saclay, Gif sur Yvette, France. His research activities are dedicated to electromechanical and magnetomechanical couplings in materials for electrical engineering applications and definition of multiscale methods for prediction of such coupled phenomena. Since 2014, he has been the Director of the Automotive Mechatronics Chair, a partnership between Centrale Supélec, Esigelec and automotive company Forvia.



France. His research interests include design, modeling and control of smart materials based actuators.